International Journal of Nanomedicine

Dovepress
open access to scientific and medical research

Open Access Full Text Article

ORIGINAL RESEARCH

Glucose-coated Berberine Nanodrug for Glioma Therapy through Mitochondrial Pathway

This article was published in the following Dove Press journal:
International Journal of Nanomedicine

Shubin Wang,[1,*] Juan An,[2,*] Weiwei Dong,[3,*] Xin Wang,[4] Jianqiu Sheng,[4] Yan Jia,[4] Yuqi He,[4] Xianzong Ma,[4] Jiheng Wang,[4] Dedong Yu,[1] Xiuqin Jia,[1] Bingyu Wang,[5] Wenbo Yu,[5] Kejia Liu,[5] Yuanyuan Zhao,[6] Yun Wu,[1] Wei Zhu,[1] Yuanming Pan[1,4,6]

[1]Department of Oncology, Baotou City Central Hospital, Baotou 014040, People's Republic of China; [2]Department of Basic Research Medical Sciences, Qinghai University, Xining 810001, People's Republic of China; [3]Department of Oncology, General Hospital of Chinese People's Liberation Army, Beijing 100085, People's Republic of China; [4]Department of Gastroenterology, The 7th Medical Center of Chinese PLA General Hospital, Beijing 100700, People's Republic of China; [5]Yidu Cloud (Beijing) Technology Co. Ltd 8F, Health Work, Beijing 100083, People's Republic of China; [6]National Center for Nanoscience and Technology, Zhongguancun, Beijing 100190, People's Republic of China

*These authors contributed equally to this work

Correspondence: Yuanming Pan
National Center for Nanoscience and Technology, Zhongguancun, Beijing 100190, People's Republic of China
Tel +86-10-6406-9831
Fax +86-10-6401-2266
Email panym@nanoctr.cn

Wei Zhu
Department of Oncology, Baotou City Central Hospital, Baotou, Inner Mongolia 01404, People's Republic of China
Tel +86-472-6955473
Fax +86-472-6955708
Email 18686111667@163.com

Introduction: Glioma is the primary malignant brain tumor with poor prognosis. Berberine (BBR) was the potential drug for anti-tumor in glioma cells. Based on its limitation of poor aqueous solubility and instability, little information of BBR nanoparticles is reported in glioma.

Methods: Different solutions including 5% glucose, 1*PBS, ddH_2O, 0.9% NaCl, cell culture medium were selected, and only 5% glucose and ddH_2O exhibited BBR-related nanoparticles. After heating for a longer time or adding a higher concentration of glucose solution, BBR nanoparticles were detected by TEM analysis. The uptake of BBR-Glu or BBR-Water nanoparticles were detected by immunofluorescence analysis for BBR autofluorescence. Cell viability was measured by MTT assay and Western blotting analysis. Apoptosis was performed with flow cytometric analysis and was detected by cleaved caspase-3 immuno-fluorescent staining. Cell cycle was used by flow cytometric analysis. Cytoskeleton was observed by confocal analysis using the neuron specific Class III ß-tubulin and ß-tubulin antibodies. Mitochondrial-related proteins were detected by Western blotting analyses and mito-tracker staining in live cells. Mitochondrion structures were observed by TEM analysis. ROS generation and ATP production were detected by related commercial kits. The tracking of BBR-Glu or BBR-Water nanoparticles into blood–brain barrier was observed in primary tumor-bearing models. The fluorescence of BBR was detected by confocal analyses in brains and gliomas.

Results: BBR-Glu nanoparticles became more homogenized and smaller with dose- and time-dependent manners. BBR-Glu nanoparticles were easily absorbed in glioma cells. The IC_{50} of BBR-Glu in U87 and U251 was far lower than that of BBR-Water. BBR-Glu performed better cytotoxicity, with higher G2/M phase arrest, decreased cell viability by targeting mitochondrion. In primary U87 glioma-bearing mice, BBR-Glu exhibited better imaging in brains and gliomas, indicating that more BBR moved across the blood–brain tumor barrier.

Discussion: BBR-Glu nanoparticles have better solubility and stability, providing a promising strategy in glioma precision treatment.

Keywords: berberine, glioma, glucose-nanocarrier, nanoparticles, mitochondria

Introduction

Glioma is the most malignant type of primary brain tumor with highly invasive phenotype, making the complete surgical resection impossible. Despite the advances in surgery, chemotherapy, and radiotherapy, the prognosis of glioma patients is far from desirable, especially for those with unresectable tumor or multifocal tumor. Therefore, exploration of novel therapy is urgently required.[1,2] Berberine (BBR) is a natural compound isolated from Chinese herbs such as Coptis

root (Huang Lian) and Amur Corktree (Huang Bai), possessing wide pharmacological effects such as antidiarrheal, antimicrobial, antioxidative and antiinflammatory, antitumor etc.[3,4] However, due to its hydrophobic properties, poor stability and bioavailability of BBR, its application was limited, and the pre-clinical potential value in glioma therapy was still unclear.

With unique properties, nanodrugs have attracted great interest. The target delivery,[5–7] controllable release,[8,9] lower systematic toxicity[10] and higher drug bioavailability,[11,12] these functions reveal a new chapter in medicine transformation. Assembling into a nanocarrier, an insoluble drug can form a nanodrug, which is the most powerful strategy.[13,14] However, safety issues like potential bio-toxicity, unknown metabolites, and great uncertainty during the use of nanocarriers still remain.[15,16] Thus, a "green" method without "toxic" nanocarrier or solvents to create a stable BBR nanoformulation is recommended and proposed in this study.[17]

BBB forms a physical separation between circulating blood and the brain parenchyma and consists of tight junctions around endothelial cells surrounded by basement membrane. It prevents pathogens and large hydrophilic molecules from entering the brain, while allowing transport of substances needed by the central nervous system (CNS) such as glucose, fatty acids, and vitamins. Here, the most challenge for BBR or other therapeutics in glioma is crossing the BBB. Fortunately, glucose-coated nanodrugs and fructose-coated nanoparticles can provide 10 to 100-times more uptake by tumor cells in various models.[18] This is probably due to the high level of glucose transporter at the surface of tumors, associated with cancer stem cells and cancer metastasis.[19] Moreover, glucose coating acts as the promising strategy for drugs to cross the BBB,[20,21] which has an important potential application for glioma treatment.[18,22] Moreover BBR, as an alkaloid, was reported to cross the BBB. Its efficacy has been investigated in various disease models of the CNS, which can be detected in the hippocampus and cerebrospinal fluid (CSF).[23–26]

In this study, a 5% glucose solution was used to dissolve BBR. Based on the easy common operation in clinic, BBR-Glu nanoparticles can be obtained. With improved solubility of BBR, this nanoformulation showed a higher inhibition than BBR in distilled water for glioma treatment, with more BBR accumulated in mitochondrion of glioma cells, the disappearance of mitochondrial cristae, adenosine-triphosphate (ATP) production, reactive oxygen species (ROS) generation, apoptotic-related proteins (Bax, Bcl-2, Cyto-C, cleavage caspase-3), and higher mitochondrial membrane potential leading to early apoptosis, cell cycle arrest and decreased cell colonies.

Experimental Methods

Chemical Reagents and Preparation

Trypsin, streptomycin, penicillin and berberine (BBR) were purchased from Sigma Chemical Co. (St. Louis, MO, USA), Dulbecco's modification of Eagle's medium (DMEM) with high-glucose concentration 4.5 g/L, 10% fetal bovine serum (FBS) and L-glutamine were ordered from Hyclone Laboratory (GE Healthcare Life Sciences, Logan). Berberine was dissolved in 5% glucose injection (BBR-Glu) or distilled water (BBR-Water) at 68°C (heated for four hours) with the final concentration of 5 mM. The stocking solution was stored at room temperature. Meanwhile, the solubility and stability of BBR was observed in other solution, such as 1*phosphate buffered solution (1*PBS), physiological saline (0.9% NaCl), cell culture medium (DMEM) under the same conditions. The following antibodies, cytochrome C (Cyto-c), Bax, Bcl-2, cleavage caspase-3 and Tuj1, β-tubulin, and β-actin, were purchased from Cell Signaling Technology (Danvers, MA, USA).

Physical Analyses of BBR-Glu Characterization

The morphology, nanoparticle size and zeta potential of BBR dissolved in distilled water or BBR-Glu solution were further analyzed (Zetasizer Nano ZS90, Malvern Instruments, UK). Ultraviolet-visible (UV-Vis) spectra were performed in the range between 200 and 800 nm by using a T80 spectrophotometer (PG Instrument Ltd, Leicester, UK). Optical spectra were obtained by measuring the absorption of the solution in a quartz cuvette with a 1 cm optical path. The optical properties were monitored for up to two weeks to test the solution stability. Transmission electron microscopy (TEM) observations were performed by a Hitachi 7700, at 100 kV (Hitachi High Technologies America Inc., Dallas, TX, USA). The specimens were prepared for TEM observation by placing small droplets of BBR-Glu or BBR-Water onto standard carbon supported 600-mesh copper grids and drying slowly in the air naturally.

Immunofluorescence Staining

Cells were cultured with medium contain BBR-Glu (50 μM) or 5% glucose solution for 48 h. Primary

monoclonal antibodies for β-tubulin (1:300 dilution) and anti-rabbit-biotinylated secondary antibody fluoreseine isothiocyanate (FITC) (Molecular Probes Inc., Eugene, OR, USA) (1:100 dilution) were used. Mitochondria was stained by mito-tracker probe from Invitrogen (M22426, MitoTracker® Deep Red FM, Invitrogen, Excitation, 644 nm, Emission, 665 nm). The nuclei of live cells were stained by Hoechst 33,342 (excitation: 350 nm, emission: 461 nm, Appligen Co., Ltd, Beijing, China), and the nuclei of fixed cells were stained with 4',6-diamidino-2'-phenylyndole (DAPI) (excitation: 358 nm, emission: 461 nm, Appligen., Co.,Ltd, Beijing, China), immunofluorescence images were recorded using a confocal laser scanning microscope (TCS SP2, Leica Microsystems AG, Wetzlar, Germany) equipped with a 630 × oil immersion objective.

Absorption of BBR-Glu or BBR-Water Nanoparticles

Specimens (BBR-Glu and BBR-Water nanoparticles) were dispersed and attained at the final concentration of 0.5 μM. The fingerprints of BBR have four peaks using UV-VIS spectroscope (Jasco V-750, Jasco, Tokyo, Japan, range: 200–800 nm). The absorption spectrum exhibits three bands with maxima around 220–350 nm, which are strong in nature, and another relatively weak band at about 422 nm. The same results were detected in BBR-Glu solution using UV-Vis absorption spectra of BBR in 5% glucose solution.

Cell Lines and Cell Culture

Human glioma U251 cells and U87 cells were obtained from the American Type Culture Collection (Manassas, VA, USA) and cultured as monolayers in DMEM supplemented with 10% FBS, 100 IU/mL penicillin, and 100 mg/mL streptomycin (Invitrogen, Carlsbad, CA, USA). Cells were maintained in an incubator with a humidified atmosphere of 5% Carbon dioxide (CO_2) at 37°C. Cells were seeded on cover slips and exposed to different types of solutions (Glu, BBR-Glu and BBR-Water). Four concentrations of BBR-Glu solution (0, 25, 50, 100 μM) in glioma cells were prepared and used for observing cell viability and apoptosis analyses using FITC-annexin-V/propidium iodide (PI) (FITC: excitation: 495 nm, emission: 520 nm; PI: excitation: 533 nm, emission: 617 nm).

Measurement of BBR Uptake and Subcellular Location

Glucose or BBR-Water (50 μM) and BBR-Glu nanoparticles were added to U251 and U87 cells for 48-h treatment. BBR-Glu and BBR emitted a yellowish fluorescence (excitation: 488 nm, emission: 564 nm), and its uptake was examined using flow cytometer and confocal microscopy. The cells were treated with BBR-Glu (50 μM) for 24 h, then incubated with mito-tracker probe at 37°C for 30 min. Cells were digested with trypsin-ethylene diamine tetraacetia acid (EDTA) and washed three times with cold 1*PBS, BBR autofluorescence was imaged using 488 nm excitation and 564 nm emission. U251 or U87 cells were detected under 200× magnification using a fluorescent microscope with a 488 nm/564 nm excitation filter.

Cellular Viability Assay

MTT assays were performed in a 96-well plate format to assess cytotoxicity of the BBR-Glu or BBR-Water particles on glioma cells, U251 and U87. Cells were seeded at a concentration of 5×10^3 cells in 96-well plates for 24 h prior to drug plus. Cells were washed and medium containing BBR-Glu (50 μM) or BBR (50 μM) and the negative control, 5% glucose solution for 48 h, respectively. Or cells were cultured with different concentrations (0, 25, 50, 100 μM) of BBR-Glu nanoparticles for five days. After incubation, the medium was removed from all wells and mediums with 0.5 mg/mL 3-(4,5-Dimethylthiazol-2-yl)-2,5- diphenyl-tetrazolium bromide (MTT, Sigma-Aldrich) was added to each well. The plate was incubated for three hours, the solution carefully aspirated from the well and 100 μL of dimethyl sulfoxide (DMSO, Sigma-Aldrich, USA) was added to each well. The plate was placed on an orbital shaker for 10 minutes and absorbance was read at 540 nm with a reference at 650 nm serving as the blank on a plate reader. The percentage of cell viability was calculated using the following formula: percentage cell viability = (OD of the experiment samples/OD of the control)×100%.

Flow Cytometric Analysis of Apoptosis

Apoptosis was evaluated by using an FITC-conjugated annexin V/PI assay kit (Invitrogen, USA) following the protocol of instruction. Briefly, cells treated with BBR-Glu or BBR-Water nanoparticles (50 μM) for 48 h respectively, were collected and washed in ice-cold PBS, and re-suspended in the annexin V-FITC and 1 μg/mL PI reagent

in the dark for 20 minutes. Labeling was analyzed by flow cytometry with a FACSCalibur™ flow cytometer (BD Biosciences, San Jose, CA). A minimum of 10,000 cells per sample were analyzed. Apoptosis was then determined and analyzed for three independent experiments. Based on the most overlap between FITC immunofluorescence and BBR auto-fluorescence, we also detected cleavage caspase-3 using laser scanning confocal microscopy by Rhodamine-labeled secondary antibody.

Cell Cycle Analysis

Cells (0.5×10^6) treated with different doses of BBR-Glu solutions (0, 25, 50, and 100 μM) for 48 h and untreated parent cells were harvested using 0.25% Trypsin-EDTA solution. The digested cells were fixed gently (drop by drop) with precooled 70% ethanol (in PBS) and were kept overnight at −20°C, then were resuspended in PBS containing 40 μg/mL PI, 0.1 mg/mL RNase (Sigma, USA) and 0.1% Triton X-100 for 30 min. Cells were washed twice using cold 1*PBS. Cell cycle was then determined and analyzed using an imaging flow cytometer (BD Accuri™ C6 software, USA).

Clonogenic Assay

The effect of BBR-Glu and BBR-Water nanoparticles on colony-forming ability was assessed by using a clonogenic assay. A total of 2000 cells were seeded into six-well trays with culture medium. Cells were exposed to BBR-Glu (50 μM), BBR-Water (50 μM) or negative control (5% glucose solution) and grown for three weeks, and fixed and stained with crystal-violet. Plates were then counted in five different fields, and images were recorded by microscopy (100× magnification).

ATP Hydrolysis Assay

A continuous ATP hydrolysis assay was applied to measure the specific ATP hydrolysis activity of all ATP synthase constructs (Beyotime Co., Ltd, Jiangsu Province, China). In this assay, ATP was constantly regenerated by an enzymatic reaction, while the consumption of nicotinamide adenine dinucleotide (NADH) was measured spectroscopically at 340 nm. The change in absorbance was measured for 250 seconds at two-second intervals at 37°C after adding 50 μg of protein complex to 1 mL reaction solution (25 mM N-2-hydroxyethylpiperazine-N-ethane-sulphonicacid (HEPES) pH 7.5, 25 mM potassium chloride (KCl), 5 mM magnesium chloride ($MgCl_2$), 5 mM potassium cyanide (KCN), 2 mM phosphoenolpyruvate, 2 mM ATP, 0.5 mM NADH, 30 units L-lactic acid dehydrogenase, 30 units pyruvate kinase), and its activity was derived by fitting the initial linear section of the slope.

Western Blotting Analysis

Western blot analysis (the amount of protein used for each sample was 40 μg) was performed in different groups (50 μM BBR-Glu, 50 μM BBR-Water, 5% glucose solution as the negative control treated for 48 h in glioma cells). Equal amounts of protein were separated by sodium dodecyl sulfate polyacrylamide gel electrophoresis SDS-PAGE) and electro-transferred onto a polyvinylidene fluoride (PVDF) membrane (Invitrogen, USA). Nonspecific antibody binding was blocked by incubation of the blots with 4% bovine serum albumin (BSA) in 1*PBS for one hour at room temperature. The blots were then probed with appropriate dilutions of primary antibodies (1:600 dilution). Then, the blots were stripped and re-probed with other antibodies against β-actin to ensure equal loading and transfer of proteins.

Glucose-coated BBR Observation and Characterization in Tumor-bearing Mice

For BBR-Glu or BBR-Water nanoparticles tracking into BBB experiments in animal models by tail vein injection for three days. The optical fluorescence of BBR was detected by (maximum excitation peak at 488 nm, and peak emission at 564 nm). Briefly, BBR-Glu (100 μL) or BBR-Water (100 μL) probe solution was injected into five glioma-bearing mice respectively by tail-vein injection for three consecutive days. Another five mice received an equal volume of 5% glucose solution at the same time. After three days, these mice were sacrificed to observe the comparation of BBR staining in the brains of different groups. These mice were obtained from the Animal Center of the Chinese Academy of Science and all animal experiments were approved by the Ethical Committee of National Center for Nanoscience and Technology, as well as Baotou Central Hospital. All the protocols were performed under the Chinese Academy of Sciences guidelines followed for the welfare of laboratory animals. In the study, the images and semiquantitative results of BBR staining were acquired using a live imaging system (CRi Maestro, PerkinElmer, USA) from the brains and tumors. The frozen glioma and brain sections were observed in the presence of BBR nanoprobes by a confocal laser

microscopy (λex: 488 nm, λem: 564 nm, red pseudo-color, Leica TCS SP5 laser scanning microscope system, Leica Microsystems, DE). Slices showing nuclear staining by 4′,6-diamidino-2-phenylindole (DAPI, Eugene, OR, USA) were examined and photographed under a confocal laser microscopy (λex: 340 nm, λem: 488 nm).

Measurement of Reactive Oxygen Species

Glioma cells were seeded and cultured for 48 h in six-well plates in the presence or absence of BBR-Glu (50 μM) nanoparticles and incubated with 10 μM of the fluorescent probe 2′,7′-dichlorofluorescein diacetate (DCFDA) for one hour. After removing the supernatant, glioma cells were trypsin-digested, collected, and washed twice with cold (1*PBS, pH 7.4), the intensity of DCFDA fluorescence (excitation: 488 nm, emission, 525 nm, Beyotime, Co., Ltd, Jiangsu, China) was then detected using a FACScan flow cytometer (Becton Dickinson, Sunnyvale, CA, USA). Briefly, the cells were incubated in PBS containing 5 μM H_2DCFDA for 15 min in the dark, cells were then washed, and intracellular fluorescent signals were acquired and quantified using IN Cell Analyzer 2000 Software (GE Healthcare). The level of ROS is presented as relative fluorescence units.

Statistical Analysis

The data shown are a summary of the results from at least three experiments and are presented as Mean ± SD. Statistical evaluation of the results was performed by one-way analysis of variance (ANOVA). The results were considered significant at a value of $p<0.05$.

Results and Discussion

Green, Safety Preparation and Characterization of BBR-Glu Nanodrug

As we known, BBR is an isoquinoline alkaloid isolated from a variety of Chinese herbs including Coptidis rhizome and Amur corktree bark (Figure 1A). Its insolubility, poor stability causes low bioavailability by oral administration and could not be used by vein injection. Through simply dissolving BBR into 5% glucose solution, BBR formed nanosized shape. This nanoformulation is much more superior to traditional chemical modification. Here glucose not only acts as the stabilizer, but also the safe and nutritious agent widely used in brain diseases. As shown in Figure 1B, stable nanoparticles can only be obtained when BBR is dissolved in 5% glucose. It was also found that BBR can be dissolved in distilled water (BBR-Water, Milli-Q Advantage A10, 18.2 MΩ.cm, Millipore, Merck, USA), but BBR solubility is highly dependent on temperature. Hence, this dissolved system cannot be stable. Within 5% glucose injection, we obtained the stable BBR nanosystem. Meanwhile, BBR exhibited the poor solubility in 1*PBS, 0.9% NaCl and DMEMunder the same conditions (50°C warm water bathing for 45 min of BBR). Hence, we further analyzed the particle size of BBR in distilled water or 5% glucose solution. TEM images demonstrated the different appearances of BBR in 5% glucose solution and distilled water. BBR-Glu nanoparticles showed the size homogeneity, with the average diameter of 238 nm (size polymer dispersity index (PDI) =0.016), and kept well dispersity for more than three months under the saturated status, the mass appearance of BBR-Glu nanoparticles was further exhibited in Figure S2B, Glucose was possibly located at the surface of BBR nanoparticles (scale bar=500 nm); In distilled water, BBR particles performed different size, the average diameter was 475 nm (size PDI=0.652), and precipitated BBR crystallization was observed less than 72 h again under the same conditions. BBR-Glu nanoparticles exhibited the spherical shape, while BBR in distilled water performed the different polygon appearances, which may lead to the instability of BBR solution in water (Figure 1C). As the negative control 5% glucose solution has no nanoparticles using TEM analysis (data not shown). Zeta potential was used to evaluate the surface charge of BBR particles. As shown in Figure 1E, we designed the same final concentration of BBR (2 mM) in different solutions. BBR-Water particles show strong positive charge in distilled water (+12.1 mV), which is due to the ionization of BBR formed positive charge. BBR-Glu nanoparticles show weak positive surface charge (+2.93 mV), because of glucose on the surface of BBR-Glu nanoparticles. UV spectra of BBR-Glu nanoparticle show four peaks at 228, 246, 353, and 422 nm (same as BBR-Water), implied the well physiochemistry properties of BBR in BBR-Glu particles system (Figure 1D). The obtained BBR-Glu nano-system was further evaluated on typical glioma cell lines U251 and U87. Furthermore, we also found the dynamic change of BBR nanoparticles in different concentrations of glucose solutions and at different times (Figure S3). Rotation with a small motor rotor and heating at 68°C at different time in 5% glucose solution (15 min, 30 min, 1 hour, 3 hours), the appearance of BBR was changed from tiny fibers to less polygonal and smaller size, When in various concentrations of glucose solution (ddH_2O, 0.1% Glu, 1% Glu, 5% Glu) for 2 hours, BBR nanoparticles became homogenized and

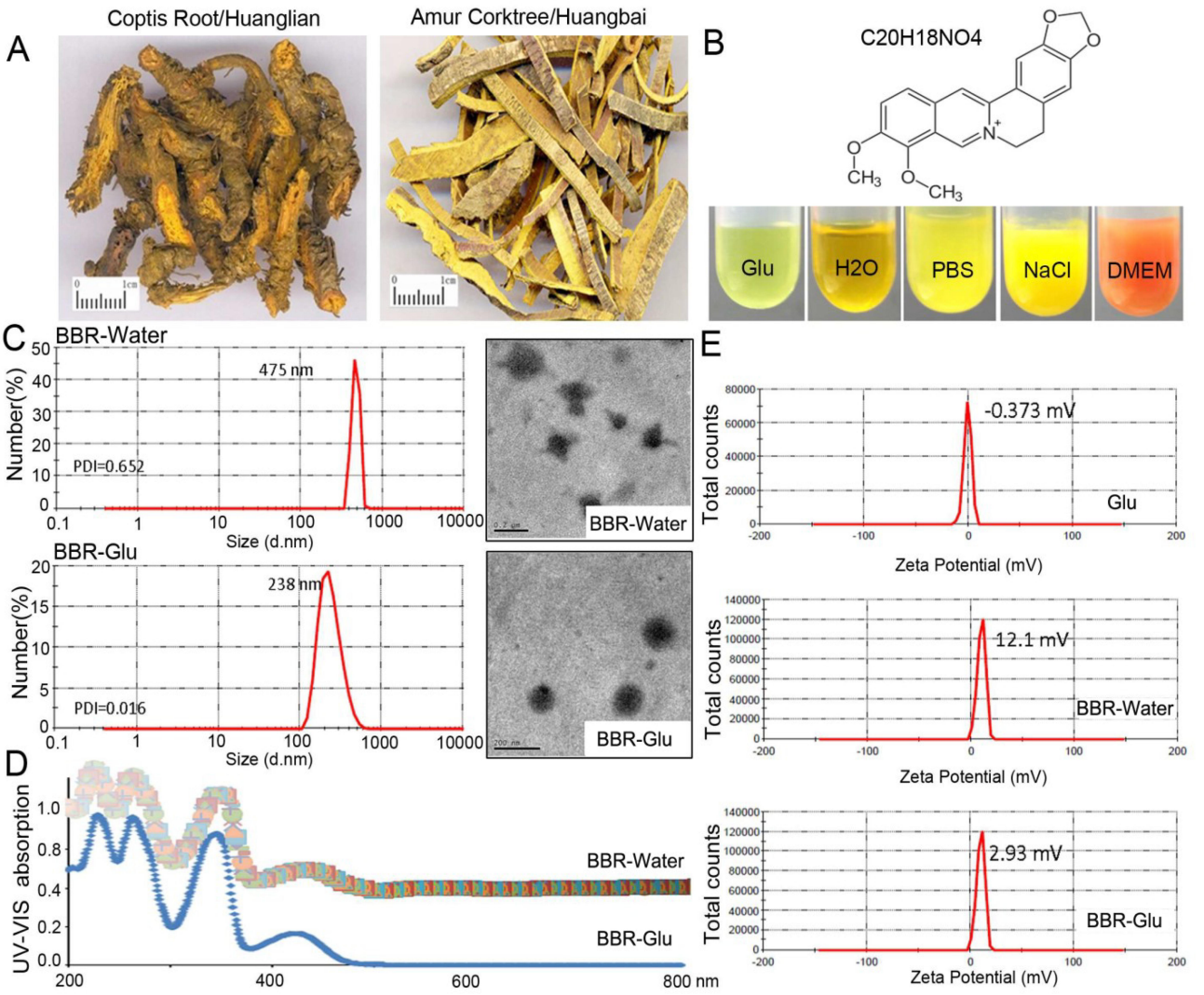

Figure 1 Unique physicochemical property of BBR-Glu nanodrug. (**A**) BBR is an isoquinoline alkaloid isolated from a variety of Chinese herbs including Coptidis rhizome and Amur Corktree bark. (**B**) Chemical structure of BBR, and it was dissolved in different solvents. (**C**) Transmission electron microscopy (TEM) images demonstrated the different appearances of BBR in 5% glucose solution and distilled water. BBR-Glu nanoparticles showed the homogeneity of size, with the average size of 238 nm (diameter, size PDI=0.016), and keep BBR stable dispersibility more than three months under the saturate status. In the distilled water, BBR-Water particles performed the heterogeneity of the size, the average size was 475 nm (diameter, size PDI=0.652), and precipitated BBR crystallization less than 72 h again under the same conditions. The former nanoparticles showed spherical shapes, the latter with different polygon shapes, which could lead to the instability of BBR particles. (**D**) BBR-Glu nanoparticle absorption spectrum characterized by four peaks at 228, 246, 353, and 422 nm using a UV-Vis absorption spectrometer, similar to the one in BBR-Water solution. (**E**) Zeta potential detection in BBR-Glu, BBR-Water and 5% glucose solution.

smaller. TEM data indicated the real size of BBR nanoparticles dissolved in different solutions for two hours. The more stability and spherical appearance of BBR-Glu nanoparticles were compared to BBR-Water nanoparticles for two weeks at room temperature.

Improved Efficacy of BBR-Glu to Glioma Cells in vitro

BBR-Glu nanoparticles show more toxicity in U87 and U251 cells. Firstly, a significant reduction of cell viability was observed in a dose-dependent manner, and the IC_{50} value of BBR-Water was 75.4 μM, while it was 25.7 μM for BBR-Glu nanoparticles at 48 h in U251 cells. In U87 cells, the IC_{50} of BBR-Glu was 19.5 μM, much lower than 87.9 μM BBR-Water at 48 h. Higher cytotoxicity of BBR-Glu, BBR-Water and 5% glucose solution in U251 and U87 glioma cells was further confirmed. Cell viability was assayed by the same BBR concentration (50 μM) addition in a time-dependent manner (Figure 2A and B and Supplementary Figure S1A), the antiproliferation ability of BBR-Glu nano-system was 1.85 times higher than in BBR-Water system. Furthermore, growth inhibition of U251 cells treated with BBR-Glu (50 μM), BBR-

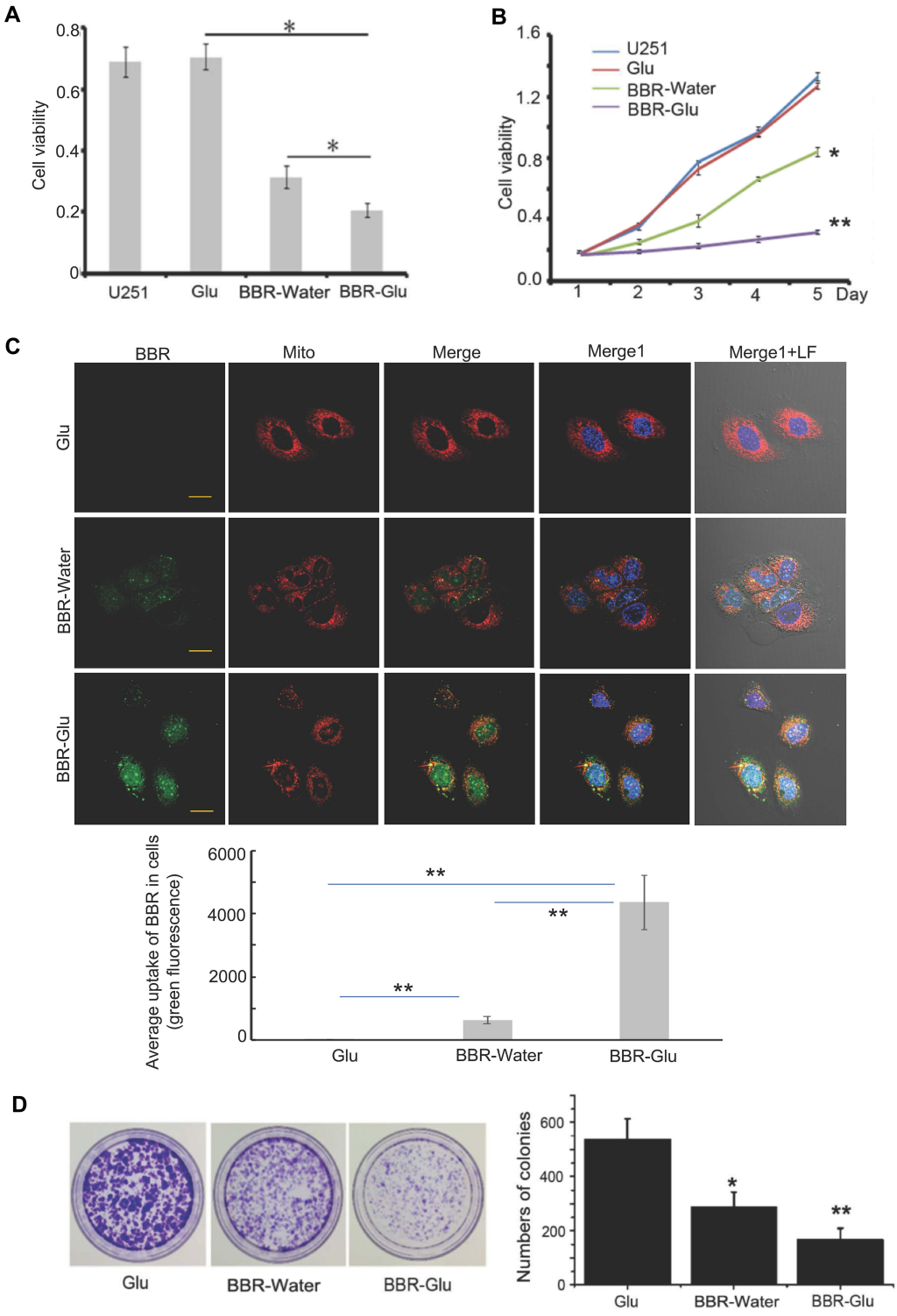

Figure 2 More uptake and cytotoxicity of U251 glioma cells treated by BBR-Glu nanodrug. Different cytotoxicity of BBR-Glu, BBR-Water, 5% glucose group in U251 glioma cells. (**A**) Effect of BBR-Glu, BBR-Water and 5% glucose (Glu) group in cell viability of human glioma U251 cells for 48 h. (**B**) Growth curve of U251 cells treated with BBR-Glu (50 μM), BBR-Water (50 μM) and Glu solution for five days. (**C**) BBR-Glu enhanced the uptake of BBR in U251 cells using flow cytometer (BBR fluorescence: excitation peak at 488 nm, and peak emission at 564 nm). More uptaken BBR localized in mitochondria was observed in BBR-Glu solution compared with that in BBR-Water or Glu solution using laser scanning confocal microscopy (scale bar=10 μm). (**D**) Different effects of BBR-Glu, BBR-Water and Glu solution on cell colonies (4× magnification). Error bars indicate standard deviation(SD), each point represents Mean ± SD of three experiments. *p<0.05, **p<0.01.

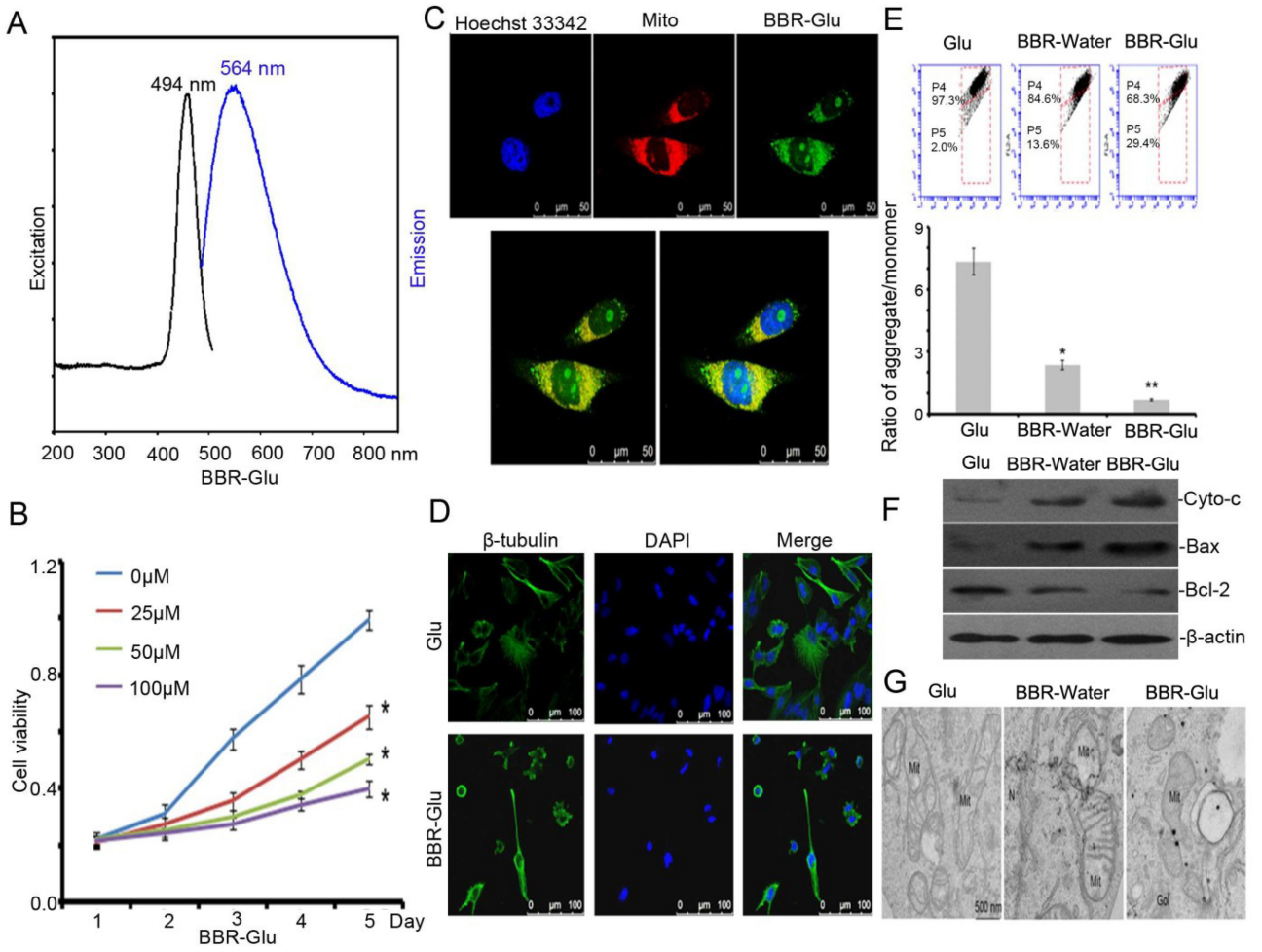

Figure 3 BBR-Glu nanodrug effects on the regulation of mitochondria in U251 glioma cells. (**A**) BBR-Glu nanoparticle exhibited the excitation max peak (494 nm) and emission max peak (564 nm). (**B**) BBR-Glu solution (50 μM) suppressed cell viability with dose-dependent manner in U251 cells for five days. (**C**) BBR-Glu (50 μM) nanoparticles co-localized in mitochondria at 48 h using confocal microscopy. (**D**) Effects of BBR-Glu (50 μM), 5% glucose solution in cytoskeleton modification by staining β-tubulin at 48 h. (**E**) BBR-Glu (50 μM), BBR-Water (50 μM) solution decreased mitochondria membrane potential by JC-1 detection in U251 cells for 48 h. The ratio of the aggregate/monomer was decreased apparently in BBR-Glu (50 μM), compared with BBR-Water (50 μM) and Glu group. (**F**) Mitochondria related apoptotic-proteins was detected in BBR-Glu (50 μM), BBR-Water (50 μM) and 5% glucose treatment in U251 cells, including the levels of Cyto-c, Bcl-2, Bax expression by Western blot analyses. (**G**) TEM images exhibited the structure of mitochondria treated by BBR-Glu (50 μM), BBR-Water (50 μM) and Glu solution for 48 h. Error bars indicates SD, each point represents Mean±SD of three experiments. *p<0.05, **p<0.01.

Water (50 μM) and 5% glucose solution for 5 days, more cytotoxicity was analyzed using BBR-Glu nanoparticles than other groups by MTT assay, 2.59 times higher efficiency was detected in BBR-Glu nanosystem compared with that in BBR-Water at the fifth day (p<0.01, Figure 2B). Similar results were identified by another glioma cell line, U87 (Supplementary Figure S1A). These results implied a higher uptake of BBR in U251 cells and U87 cells treated by BBR-Glu nanoparticles. Using BBR's green fluorescence, with maximum excitation peak at 488 nm, and peak emission at 564 nm (Figure 3A), the uptake of BBR-Glu nanoparticles were used by flow cytometer and laser scanning confocal microscopy analyses, 8.2 times more uptake of BBR-Glu nanoparticles were confirmed in glioma U251 cells using flow cytometer and more co-localization with mitochondrion using laser scanning confocal microscopy (Figure 2C). Cell colonies were apparently decreased in the BBR-Glu group compared with those in the BBR-Water group and 5% glucose solution (p<0.05, Figure 2D). Furthermore, BBR-Glu solution suppressed cell viability with a dose-dependent manner in U251 cells for five days (Figure 3B). At 48 h, more co-localization of BBR-Glu nanoparticles and mitochondria was observed in U251 cells (Figure 3C and Supplementary Figure S4). Similar results were shown in U87 cells (Supplementary Figure S2A and Supplementary Figure S4), followed by fewer formations of cell colonies in BBR-Glu solution than

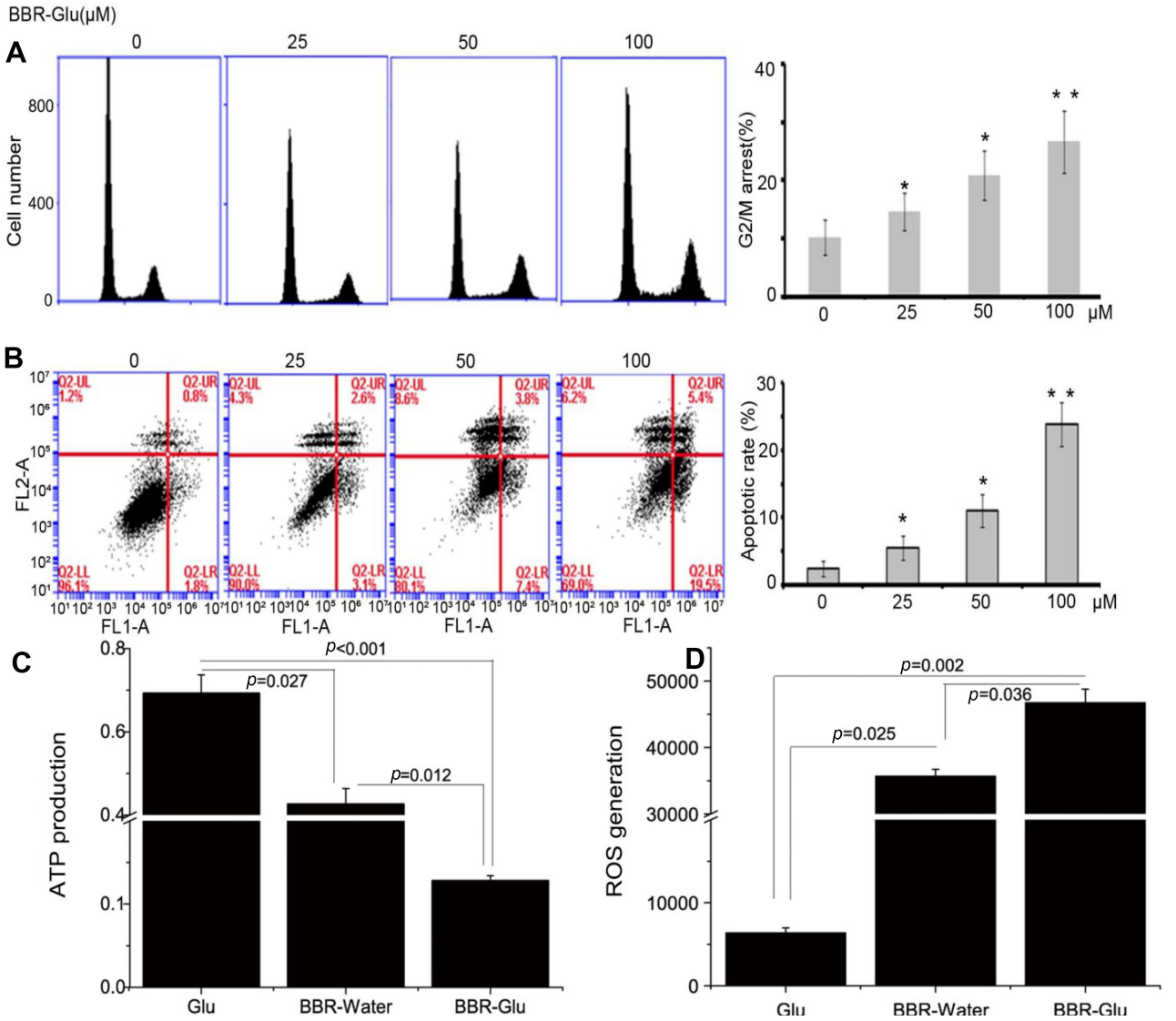

Figure 4 BBR-Glu nanodrug induced more cell cycle arrest and early apoptosis. BBR-Glu nanoparticles suppressed mitochondria-mediated early apoptosis and G2/M arrest through inducing high level of ROS generation and decreased ATP production. (**A**) BBR-Glu nanoparticles induced G2/M arrest with dose-dependent manner. (**B**) BBR-Glu nanoparticles induced high ratio of early apoptosis with dose-dependent manner. (**C**) Mitochondrial ATPase activity was suppressed by BBR-Glu solution (50 μM) at 48 h. (**D**) High level of ROS generation was induced by BBR-Glu solution (50 μM) for 48 h treatment. Each point represents Mean ± SD of three experiments. *p<0.05, **p<0.01.

BBR-Water and 5% glucose solution (Figure 2D and Supplementary Figure S1C).

Pharmacological mechanism is important for clinical instruction. Here, BBR-Glu nanodrug performed the powerful inhibition in cell proliferation by MTT assay and colony formation analysis. The underlying mechanism of BBR-Glu nanoparticles was further studied in glioma cells. It was reported that BBR anticancer ability is based on the induction of apoptosis and cell cycle arrest, as well as the inhibition of cell migration and invasion, high level of ROS generation, DNA topoisomerase inhibition, p53 activation, and NF-κB signal inactivation.[4,27–29] Early apoptosis was observed with the dose-dependent manners of BBR-Glu nanodrug, and the colocalization of BBR-Glu and mitochondria was also identified using confocal microscopy. Interestingly, BBR fluorescence and mito-tracker probe were co-localized, indicating that BBR-induced apoptosis is associated with mitochondrial dysfunction. It implied that the anticancer ability of BBR was associated with mitochondrial dysfunction, then we further analyzed the mitochondria member potential (MMP), ROS generation, ATP production and the mitochondrial structure. Reduced MMP function (Figure 3E) and mitochondrial related apoptotic proteins, including

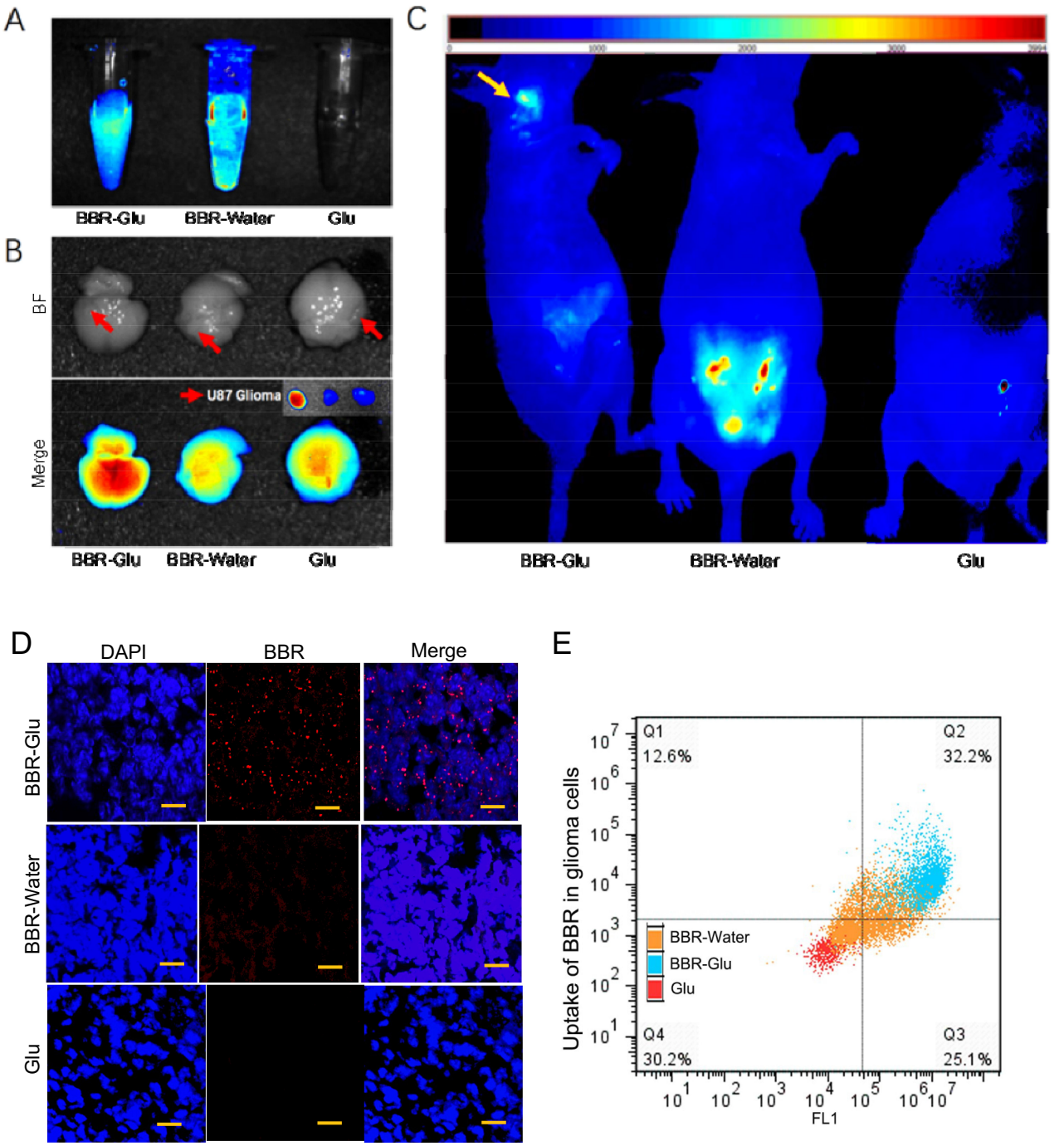

Figure 5 In live-animal optical imaging of BBR probes for specific glioma targeting. (**A**) BBR probes preparation, 5% glucose solution was the negative control. (**B**) the primary glioma-bearing brains were dissected and subjected to ex vivo optical imaging. Under the BBR fluorescent light, the gliomas were distinct from the normal brains in the mouse treated with the different BBR probes by tail-vein injection. The negative control was not visible with the BBR-Water probe in tumor. (**C**) BBR probe was observed in the head of BBR-Glu group. In the BBR-Water was obviously observed in theabdomen. The negative control was weakly visible in the abdomen as the possible background. (**D**) The optical imaging of biodistribution of BBR nanoprobes in the glioma tumor sections using confocal analysis. Immunofluorescence staining of glioma xenografts in primary brains treated with BBR-Glu, BBR-Water and Glu solutions by intravenous injection (scale bar = 50 μm). (**E**) More uptake of BBR-Glu nanoparticles was detected by flow cytometric analysis using BBR autofluorescence when digesting the fresh glioma specimens.

Bax, Cyto-c, Bcl-2 and cleavage caspase-3, high level of ROS generation and decreased ATP production exhibited in BBR-Glu group compared with others. The level of Bax, Cyto-c expression was upregulated after BBR-Glu nanodrug treatment in glioma cells, with downregulation of Bcl-2 expression and ATP generation and decreased MMP function. To investigate the mitochondrial apoptotic events involved in BBR-Glu induced apoptosis, the vital

mitochondrial dye 5,5',6,6'-Tetrachloro-1,1',3,3'-tetraethylimidacarbocyanine (JC-1) is a useful tool for investigating mitochondrial function. The dye underwent a reversible variation in fluorescence emission from green to red as the MMP increased. Cells with high membrane potential promote the formation of dye aggregates (red fluorescence) and cells with low membrane potential contain monomeric JC-1 (green fluorescence). To investigate the loss of MMP during early apoptosis induced by BBR-Glu, BBR or glucose, cells were stained with JC-1 and monitored with flow cytometry. As shown in Figure 3E, JC-1 was accumulated in negative control cells, indicating a higher mitochondrial membrane potential. In contrast, JC-1 was poorly accumulated in BBR-Glu-treated cells, indicating more disruption of MMP ($p<0.01$).

Besides, the levels of anti-apoptotic protein Bcl-2 and pro-apoptotic protein, Bax and Cyto-c were analyzed. Western blot analysis showed that the treatment of U251 and U87 cells with BBR-Glu resulted in a marked reduction of Bcl-2 expression and increased the levels of Bax and Cyto-c compared with BBR-Water and 5% glucose group (Figure 3F and Supplementary Figure S1E). These results suggest that BBR alters the levels of mitochondrial mediated apoptotic proteins of Bcl-2/Bax/Cyto-c/cleavage caspase-3 signaling pathway (Figure S7). And more BBR co-localized with mitochondria at the early stage (6 hours) in U251 and U87 cells treated with BBR-Glu solution (Figure S4). It meant that BBR-Glu nanodrug contributed easily to the treatment of glioma cells by the mitochondria-pathway. Moreover, BBR-Glu nanoparticles induced a high ratio of early apoptosis in a dose-dependent manner in glioma cells (Figure 4B).

ROS accumulation is involved in mitochondrial signaling pathways and correlated with early apoptotic signals. ROS is an important messenger molecule in energy metabolism and related apoptosis. As shown in Figure 4D and supplementary Figure S2E compared with control cells, treatment with 50 μM of BBR-Glu for 48 h, markedly increased ROS generation. The change of ATP generation was investigated to determine if it occurred via the increase of ROS generation.

Therefore, to accomplish this, U251 cells were incubated with BBR-Glu 50 μM for 48 h and the change in ATP generation was measured following the introduction of commercial kit (Beyotime Co. Ltd). As shown in Figure 4C and Supplementary Figure S2D, decreased ATP generation was detected in BBR-Glu compared with the negative control. U251 cells were treated with different solutions for 48 h, and then incubated with a cytoskeleton-specific dye β-tubulin at 37°C for 15 min. β-tubulin was accumulated in control cells, where β-tubulin displayed a bright-green fluorescence indicating cytoskeleton, whereas, the number of cells with β-tubulin decreased in the cells treated with BBR-Glu nanoparticles (Figure 3D). Furthermore, the neuron specific Class III ß-tubulin (Tuj1), was also performed to detect the cytotoxicity of BBR-Water and BBR-Glu nanoparticles. The length of cytoskeleton (Tuj1 protein) was shortened and the immunofluorescence was apparently reduced after 6 hours with 50 μM BBR-Glu addition, while the length Tuj1 protein was apparently reduced after 12 h with 50 μM BBR-Water addition, the immunofluorescence was decreased after 24 h (Supplementary Figure S5 and S6). Mitochondria and cytoskeleton damage are common causes of cell cycle arrest and apoptosis. Flow cytometry showed high percentage of apoptotic rate and increased G2/M phase ratio in BBR-Glu solution with a dose-dependent manner in glioma cells (Figure 4A and B, Supplementary Figure S1B and S1D). Furthermore, TEM images exhibited the obvious disruption of mitochondria with lacking or decreased number of cristae fragmented and shortened cytoskeleton after BBR-Glu solution treatment compared with others (Figure 3G and Supplementary Figure S2C, S5 and S6). It was implied that the higher cytotoxicity of BBR-Glu nanoparticles by targeting mitochondria pathway and cytoskeleton in glioma cells.

BBR-Glu as the Promising Nanodrug in Primary Glioma-bearing Mice

After the surgery of glioma, commonly, intratumor injection or temozolomide oral administration is the glioma general treatment in clinic. Collectively, we will use IP administration or intratumor injection after brain resection in xenograft animal models. The administration and the final effective concentration of BBR-Glu nanoparticles should be identified in tumor-bearing animal models, which is benefit for the clinical trials in future.

It is well known that nanoparticles showed potential to cross the BBB for brain disease treatments. The mechanism of nanoparticles across the BBB is still poorly understood. It is probably that nanoparticles reassemble when they cross these barriers. Size is not the decisive factor to determine whether the nanoparticle can cross the BBB. The physicochemical and protein receptor properties (including surface charge and surface modification) influence their BBB-cross. It is important that glucose can cross the BBB, when using glucose-coated nanoparticles could re-assemble into the

brain, which probably help the BBR-Glu nanoparticles cross the barrier. Meanwhile, we also made an experiment in an orthotopic xenograft model of human glioma cells to verify whether BBR-Glu nanoparticles did cross the BBB. BBR imaging was potentially used to visualize the passive or active tumor-targeting of nanocarriers, which were brought about by the enhanced permeability and retention (EPR) effect and the incorporation of tumor-target components. The applications of BBR in live fluorescence imaging of nanocarriers were adopted in the present study. The human brain glioma cell line U87 was cultured, and then inoculated by injection with stereotactic guidance into the frontal white matter of nude mice. After 35 days the tumor had slowly grown. Mice bearing U87 xenografts in their brains were loaded with the same concentration of BBR solutions,

BBR-Glu or BBR-Water (100 μL, respectively) by tail-veil administration for three consecutive days to investigate the nanoparticle biodistribution, 5% glucose solution as the negative control (Figure 5A). The animals were sacrificed after finishing the injection protocols, and brain and tumors were examined by immunofluorescence staining. It was found that accumulation of BBR-Glu in the brain was stronger than those in other groups, which indicated that nanoparticles can increase the BBB permeability for a better penetration of drug-loaded glucose into the brain tumors (Figure 5B, D and E). BBR fluorescence images of mice bearing glioma demonstrated that the fluorescence emission of BBR in the tumor was accumulated in the brain, the other glioma xenografted mouse treated with BBR-Water was mainly observed in the abdomen (Figure 5C). Therefore, the animal experiments identified the BBR-Glu nanoparticles can cross the BBB for brain tumor treatments to some extent. We understand that more experiments in animal models may be better to reveal this phenomenon. However, in the present study, we mainly focused on in cell experiments and we did further in animal models to consolidate this conclusion.

Conclusion

Traditional nanocarrier and nanoformulation blocks the clinical translation of nanodrugs because the nanocarrier is usually not FDA approved. In addition, the nanopreparation process usually could not meet the multiple requirements involved in clinical nanodrug production, due to introduction of a toxic agent, or cannot be reproduced. In this study, a simple, green and easily operated preparation technology was developed and used for preparation of BBR-Glu nanodrug. With increased solubility and better stability, BBR-Glu nanodrugs performed enhanced cytotoxicity to glioma cells. The improved anticancer activity of the BBR-Glu nanodrug was observed through mitochondria damage and increased uptake in cell experiments and animal models (Figure 3G, Supplementary Figure S2, Figure 5D and E). Because a high level of glucose transporter was located on the surface of tumor cells and cancer stem cells, and glucose-coating strategy acts as a promising method for drug delivery across the BBB, here BBR-Glu has important potential applications for glioma treatment. A 5% glucose injection is commonly used in clinic, this concentration is also the iso-osmotic solution in the clinic treatment. Hence, it is beneficial for dissolving BBR and forming BBR-Glu nanodrugs.

This complex of BBB is a biological barrier that many drugs cannot cross because the tight junction and receptor potential channel gene expressions. Interestingly, various nanocarriers have been developed to help agents to cross this barrier. The transfer rate of glucose-coated gold nanoparticles across primary human brain endothelium[20] and similar glucose-receptor modified nanocarriers could be applied for brain research, such as novel liposome can overcome the ineffective delivery of normal drug formulations to the brain by targeting the glucose transporters (GLUT family) on the BBB.[30] And GLUT1 is crucial for the development of the BBB in vivo.[31] Moreover, in glioma cells, more GLUTs are highly expressed at the glioma cell membrane,[32] which is associated with resistance for temozolomide in vitro.[33] Moreover, the blood–brain tumor barrier (BBTB) encompasses existing and formed new blood vessels that contribute to the delivery of nutrients and oxygen to the tumor and facilitate glioma cell migration to other parts of the brain. The high metabolic demands of high-grade glioma create hypoxic areas that trigger increased expression of VEGF and angiogenesis, leading to the formation of abnormal leaky vessels and a dysfunctional BBB.[34] Some evidence supported BBR had potent antitumor activity against human and rat malignant brain tumors[31,35] and against brain injury or neurodegenerative diseases across the BBB to some extent.[36,37]

There are some important reports that have supported the glucose-coating nanoparticle as a key driver for GLUT1/3-mediated nanoparticle internalization in the BBB structure or tumor microenvironments.[18,19,21,38] They implied that glucose-coated nanoparticles can be applied for translational medicine in the future. Furthermore, BBR

was the potential drug in different brain diseases including brain tumors,[39] traumatic brain injury,[40] brain ischemia etc.[41–43] The 5% glucose injection is commonly used in clinics, this concentration is also the iso-osmotic solution in the clinic treatment. Hence, it is benefit for dissolving BBR and forming BBR-Glu nanodrug. The combination between glucose and BBR, forming the novel nanodrug, could be applied for animal models or clinical trials. However, the administration of BBR and the final effective concentration of BBR at the target site (such as glioma or brain) was still poorly understood recently. Data from animal experiments indicated that different administrations, such as intravenous (IV) injection, intraperitoneal (IP) injection, and intragastric (IG) oral administration, have the different LD_{50} of BBR in mice. The LD_{50} of BBR from IV and IP injections was 9.0386 and 57.6103 mg/kg, respectively; but no LD_{50} was found in the IG group. A significant difference in bioavailability was observed between the different routes. Furthermore, the concentration of BBR in the blood from different IG doses was also significantly different. However, the absorption of BBR by IG administration had a relative limitation. From the analysis of BBR content in the blood after various administrations, these data implied the concentration of BBR in the blood contributed to its acute toxicity, and the routes of administration might be an important factor that affected the toxicity evaluation of the BBR-Glu nanodrug.[44]

Enhancement of the permeability of the BBB led to more drugs crossiing into the brain, which was shown to be a promising strategy to improve drug absorption and treatment efficacy by nanotechniques, hyperthermia techniques, receptor-mediated transport, cell-penetrating peptides and cell-mediated delivery. Glucose-coating strategy as the nanocarrier was effective to overcome the BBB,[38,39] because glucose-coating nanoparticles was a key driver for GLUT1/3-mediated nanoparticle internalization in the BBB structure or tumor microenvironments.[18,19,38] It implied that glucose-coated nanoparticles can be applied for translational medicine in the future. Furthermore, BBR was a potential drug in different brain diseases (glioma, traumatic brain injury, brain ischemia etc).[18,33,42,43,45] A 5% glucose injection is commonly used in clinics, this concentration is also the iso-osmotic solution in the clinic treatment, hence it is beneficial for dissolving BBR and forming the promising BBR-Glu nanodrug.

Electronic Additional Files

Additional figures and figure legends were collected in the supplementary files.

Abbreviations

BBB, blood–brain barrier; BBR, berberine; BBTB, blood–brain tumor barrier; DCFDA, 2′,7′-dichlorofluorescein diacetate; EPR, enhanced permeability and retention; FITC, fluorescein isothiocyanate; GLUT, glucose transporter; IG, intragastric; IP, intraperitoneal; IV, intravenous; MMP, mitochondria member potential; PAGE, polyacrylamide gel electrophoresis; PDI, polymer dispersity index; PI, propidium iodide; PVDF, polyvinylidene fluoride; SDS, sodium dodecyl sulfate; TEM, transmission electron microscopy.

Acknowledgments

This work was supported by the China Postdoctoral Science Foundation (No. 2017M613421) to Yuanming Pan. Yuanyuan Zhao was supported by the National Natural Science Foundation of China (No. 31570968) and the Natural Science Foundation of Beijing, China (No. 7152157). Juan An was supported by the National Natural Science Foundation of China (No. 81460429), the Chunhui Plan of Ministry of Education of China (No. Z2017037) and the Applied Basic Research of Qinghai (No. 2013-Z-929Q and No.2018-ZJ-744). Yuqi He was supported by the Beijing Municipal Science & Technology Commission (No. Z171100001017145). We also thank Yiduyun for assistance in data processing.

Author Contributions

All authors made substantial contributions to conception and design, acquisition of data, or analysis and interpretation of data; took part in drafting the article or revising it critically for important intellectual content; gave final approval of the version to be published; and agree to be accountable for all aspects of the work.

Disclosure

The authors report no conflicts of interest in this work.

References

1. Van Meir EG, Hadjipanayis CG, Norden AD, Shu HK, Wen PY, Olson JJ. Exciting new advances in neuro-oncology: the avenue to a cure for malignant glioma. *CA Cancer J Clin*. 2010;60:166–193. doi:10.3322/caac.20069
2. Thakor AS, Gambhir SS. Nanooncology: the future of cancer diagnosis and therapy. *CA Cancer J Clin*. 2013;63:395–418.
3. Li-Weber M. Targeting apoptosis pathways in cancer by Chinese medicine. *Cancer Lett*. 2013;332:304–312. doi:10.1016/j.canlet.2010.07.015
4. Li W, Hua B, Saud SM, et al. Berberine regulates AMP-activated protein kinase signaling pathways and inhibits colon tumorigenesis in mice. *Mol Carcinog*. 2015;54:1096–1109. doi:10.1002/mc.22179

5. Montenegro JM, Grazu V, Sukhanova A, et al. Controlled antibody/(bio-) conjugation of inorganic nanoparticles for targeted delivery. *Adv Drug Deliv Rev*. 2013;65:677–688. doi:10.1016/j.addr.2012.12.003
6. Bhirde AA, Chikkaveeraiah BV, Srivatsan A, et al. Targeted therapeutic nanotubes influence the viscoelasticity of cancer cells to overcome drug resistance. *ACS Nano*. 2014;8:4177–4189. doi:10.1021/nn501223q
7. Zhen Z, Tang W, Chen H, et al. RGD-modified apoferritin nanoparticles for efficient drug delivery to tumors. *ACS Nano*. 2013;7:4830–4837. doi:10.1021/nn305791q
8. Ganta S, Devalapally H, Shahiwala A, Amiji M. A review of stimuli-responsive nanocarriers for drug and gene delivery. *J Control Release*. 2008;126:187–204. doi:10.1016/j.jconrel.2007.12.017
9. Junghanns JU, Muller RH. Nanocrystal technology, drug delivery and clinical applications. *Int J Nanomedicine*. 2008;3:295–309. doi:10.2147/ijn.s595
10. Fang RH, Hu CM, Luk BT, et al. Cancer cell membrane-coated nanoparticles for anticancer vaccination and drug delivery. *Nano Lett*. 2014;14:2181–2188. doi:10.1021/nl500618u
11. Xu X, Xie K, Zhang XQ, et al. Enhancing tumor cell response to chemotherapy through nanoparticle-mediated codelivery of siRNA and cisplatin prodrug. *Proc Natl Acad Sci U S A*. 2013;110:18638–18643. doi:10.1073/pnas.1303958110
12. Wei T, Liu J, Ma H, et al. Functionalized nanoscale micelles improve drug delivery for cancer therapy in vitro and in vivo. *Nano Lett*. 2013;13:2528–2534. doi:10.1021/nl400586t
13. Pelaz B, Jaber S, de Aberasturi DJ, et al. The state of nanoparticle-based nanoscience and biotechnology: progress, promises, and challenges. *ACS Nano*. 2012;6:8468–8483. doi:10.1021/nn303929a
14. Maeda H, Nakamura H, Fang J. The EPR effect for macromolecular drug delivery to solid tumors: improvement of tumor uptake, lowering of systemic toxicity, and distinct tumor imaging in vivo. *Adv Drug Deliv Rev*. 2013;65:71–79. doi:10.1016/j.addr.2012.10.002
15. Liu G, Gao J, Ai H, Chen X. Applications and potential toxicity of magnetic iron oxide nanoparticles. *Small*. 2013;9:1533–1545. doi:10.1002/smll.201201531
16. Zhao Y. Fast evolving nanotechnology and progress in the National Center for Nanoscience and Technology of China. *Adv Mater*. 2013;25:3756–3757. doi:10.1002/adma.201302796
17. Huhn D, Kantner K, Geidel C, et al. Polymer-coated nanoparticles interacting with proteins and cells: focusing on the sign of the net charge. *ACS Nano*. 2013;7:3253–3263. doi:10.1021/nn3059295
18. Hu C, Niestroj M, Yuan D, Chang S, Chen J. Treating cancer stem cells and cancer metastasis using glucose-coated gold nanoparticles. *Int J Nanomedicine*. 2015;10:2065–2077. doi:10.2147/IJN.S72144
19. Barbaro D, Di Bari L, Gandin V, et al. Glucose-coated superparamagnetic iron oxide nanoparticles prepared by metal vapour synthesis are electively internalized in a pancreatic adenocarcinoma cell line expressing GLUT1 transporter. *PLoS One*. 2015;10:e0123159. doi:10.1371/journal.pone.0123159
20. Gromnicova R, Davies HA, Sreekanthreddy P, et al. Glucose-coated gold nanoparticles transfer across human brain endothelium and enter astrocytes in vitro. *PLoS One*. 2013;8:e81043. doi:10.1371/journal.pone.0081043
21. Gromnicova R, Yilmaz CU, Orhan N, et al. Localization and mobility of glucose-coated gold nanoparticles within the brain. *Nanomedicine*. 2016;11:617–625. doi:10.2217/nnm.15.215
22. Feng G, Kong B, Xing J, Chen J. Enhancing multimodality functional and molecular imaging using glucose-coated gold nanoparticles. *Clin Radiol*. 2014;69:1105–1111. doi:10.1016/j.crad.2014.05.112
23. Simoes Pires EN, Frozza RL, Hoppe JB, Menezes Bde M, Salbego CG. Berberine was neuroprotective against an in vitro model of brain ischemia: survival and apoptosis pathways involved. *Brain Res*. 2014;1557:26–33. doi:10.1016/j.brainres.2014.02.021
24. Cui HS, Matsumoto K, Murakami Y, Hori H, Zhao Q, Obi R. Berberine exerts neuroprotective actions against in vitro ischemia-induced neuronal cell damage in organotypic hippocampal slice cultures: involvement of B-cell lymphoma 2 phosphorylation suppression. *Biol Pharm Bull*. 2009;32:79–85. doi:10.1248/bpb.32.79
25. Zhou J, Du X, Long M, et al. Neuroprotective effect of berberine is mediated by MAPK signaling pathway in experimental diabetic neuropathy in rats. *Eur J Pharmacol*. 2016;774:87–94. doi:10.1016/j.ejphar.2016.02.007
26. Abdel Moneim AE. The neuroprotective effect of berberine in mercury-induced neurotoxicity in rats. *Metab Brain Dis*. 2015;30:935–942. doi:10.1007/s11011-015-9652-6
27. Choi MS, Yuk DY, Oh JH, et al. Berberine inhibits human neuroblastoma cell growth through induction of p53-dependent apoptosis. *Anticancer Res*. 2008;28:3777–3784.
28. Li J, Gu L, Zhang H, et al. Berberine represses DAXX gene transcription and induces cancer cell apoptosis. *Lab Invest*. 2013;93:354–364. doi:10.1038/labinvest.2012.172
29. Zhao H, Halicka HD, Li J, Darzynkiewicz Z. Berberine suppresses gero-conversion from cell cycle arrest to senescence. *Aging (Albany NY)*. 2013;5:623–636. doi:10.18632/aging.100593
30. Qin Y, Fan W, Chen H, et al. In vitro and in vivo investigation of glucose-mediated brain-targeting liposomes. *J Drug Target*. 2010;18(7):536–549. doi:10.3109/10611861003587235
31. Zheng PP, Romme E, Spek PJVD, et al. Glut1/SLC2A1 is crucial for the development of the blood-brain barrier in vivo. *Ann Neurol*. 2010;68(6):835–844. doi:10.1002/ana.22318
32. Yang L, Li YM, Tian RF, et al. The expression and significance of HIF-1α and GLUT-3 in glioma. *Brain Res*. 2009;1304(1304):149–154. doi:10.1016/j.brainres.2009.09.083
33. Le Calvé B, Rynkowski M, Le Mercier M, et al. Long-term in vitro treatment of human glioblastoma cells with temozolomide increases resistance in vivo through up-regulation of GLUT transporter and aldo-keto reductase enzyme AKR1C expression. *Neoplasia*. 2010;12(9):727–739. doi:10.1593/neo.10526
34. Van TO, Yetkinarik B, de Gooijer MC, et al. Overcoming the blood-brain tumor barrier for effective glioblastoma treatment. *Drug Resist Updates*. 2015;19(10):1–12. doi:10.1016/j.drup.2015.02.002
35. Eom KS, Kim HJ, So HS, et al. Berberine-induced apoptosis in human glioblastoma T98G cells is mediated by endoplasmic reticulum stress accompanying reactive oxygen species and mitochondrial dysfunction. *Biol Pharm Bull*. 2010;33(10):1644–1649. doi:10.1248/bpb.33.1644
36. Chen CC, Hung TH, Lee CY, et al. Berberine protects against neuronal damage via suppression of glia-mediated inflammation in traumatic brain injury. *PLoS One*. 2014;9:e115694. doi:10.1371/journal.pone.0115694
37. Zhang DM, He ZW, Liu XD, et al. In-vivo and in-vitro studies on the effect of Huang-Lian-Jie-Du-Tang on nimodipine transport across rat blood-brain barrier. *J Pharm Pharmacol*. 2008;59(12):1733–1738. doi:10.1211/jpp.59.12.0017
38. Venturelli L, Nappini S, Bulfoni M, et al. Glucose is a key driver for GLUT1-mediated nanoparticles internalization in breast cancer cells. *Sci Rep*. 2016;6:21629. doi:10.1038/srep21629
39. Liu Q, Xu X, Zhao M, et al. Berberine induces senescence of human glioblastoma cells by downregulating the EGFR-MEK-ERK signaling pathway. *Mol Cancer Ther*. 2015;14:355–363. doi:10.1158/1535-7163.MCT-14-0634
40. Chai YS, Hu J, Lei F, et al. Effect of berberine on cell cycle arrest and cell survival during cerebral ischemia and reperfusion and correlations with p53/cyclin D1 and PI3K/Akt. *Eur J Pharmacol*. 2013;708:44–55. doi:10.1016/j.ejphar.2013.02.041

41. Chen W, Wei S, Yu Y, et al. Pretreatment of rats with increased bioavailable berberine attenuates cerebral ischemia-reperfusion injury via down regulation of adenosine-5′monophosphate kinase activity. *Eur J Pharmacol*. 2016;779:80–90. doi:10.1016/j.ejphar.2016.03.015
42. de Oliveira JS, Abdalla FH, Dornelles GL, et al. Berberine protects against memory impairment and anxiogenic-like behavior in rats submitted to sporadic Alzheimer's-like dementia: involvement of acetylcholinesterase and cell death. *Neurotoxicology*. 2016;57:241–250. doi:10.1016/j.neuro.2016.10.008
43. Sedaghat R, Taab Y, Kiasalari Z, Afshin-Majd S, Baluchnejadmojarad T, Roghani M. Berberine ameliorates intrahippocampal kainate-induced status epilepticus and consequent epileptogenic process in the rat: underlying mechanisms. *Biomed Pharmacother*. 2017;87:200–208. doi:10.1016/j.biopha.2016.12.109
44. Kheir MM, Wang Y, Hua L, et al. Acute toxicity of berberine and its correlation with the blood concentration in mice. *Food Chem Toxicol*. 2010;48:1105–1110. doi:10.1016/j.fct.2010.01.033
45. Zou H, Long J, Zhang Q, et al. Induced cortical neurogenesis after focal cerebral ischemia–Three active components from Huang-Lian-Jie-Du Decoction. *J Ethnopharmacol*. 2016;178:115–124. doi:10.1016/j.jep.2015.12.001